Tellus
SERIES A
DYNAMIC
METEOROLOGY
AND OCEANOGRAPHY
PUBLISHED BY THE INTERNATIONAL METEOROLOGICAL INSTITUTE IN STOCKHOLM

*Tellus (2009), 61A, 579–586*
*Printed in Singapore. All rights reserved*



TELLUS

# Intermediate time error growth and predictability: tropics versus mid-latitudes

*By* DAVID M. STRAUS[1]* and DAN PAOLINO[2], [1]*George Mason University MSN 6A2, Fairfax, VA 22030, USA;* [2]*Center for Ocean-Land-Atmosphere Studies, 4041 Powder Mill Rd. Suite 302, Calverton, MD 2075, USA*

(Manuscript received 10 March 2009; in final form 1 June 2009)

ABSTRACT

The evolution of identical twin errors from an atmospheric general circulation model is studied in the linear range (small errors) through intermediate times and the approach to saturation. Between forecast day 1 and 7, the normalized error variance in the tropics is similar to that at higher latitudes. After that, tropical errors grow more slowly. The predictability time $\tau$ taken for tropical errors to reach half their saturation values is larger than that for mid-latitudes, especially for the planetary waves, thus implying greater potential predictability in the tropics.

The discrepancy between mid-latitude and tropical $\tau$ is more pronounced at 850 hPa than at 200 hPa, is largest for the planetary waves, and is more pronounced for errors arising from wave phase differences (than from wave amplitude differences).

The spectra of the error in 200 hPa zonal wind show that for forecast times up to about 5 d, the tropical error peaks at much shorter scales than the mid-latitude errors, but that subsequently tropical and mid-latitude error spectra look increasingly similar.

The difference between upper and lower level tropical $\tau$ may be due to the greater influence of mid-latitudes at the upper levels.

## 1. Introduction

Many theoretical and model studies of atmospheric predictability have tended to focus either on the initial growth of differences in solutions which originate from nearly identical initial conditions, or on the predictability of time means due to anomalies in the slowly evolving components of the climate system such as ocean and land. These approaches represent limiting cases of very small or very large time, and allow for simplifying assumptions. The first case allows for the use of linear (or linearized) dynamics, while the second allows the use of a steady-state assumption.

The growth of initially small differences (also called errors) once they outgrow the linear phase is a more complex problem, and general results are hard to obtain. One approach that has made a great deal of headway in describing intermediate error growth in general terms is turbulence theory, in which the drastic assumptions of isotropy and homogeneity allow for a universal depiction of the (ensemble averaged) error growth at all stages, given only the spatial spectrum of the background flow (Lorenz, 1969; Leith and Kraichnan, 1972; Rotunno and Snyder, 2008).

The real atmosphere is of course an example of highly inhomogeneous turbulence, with tropical and extratropical regimes dominated by quite distinct types of instability and wave motions. In the extratropics, a wide range of baroclinic and barotropic instabilities lead to rapid initial error growth, while one example of the dynamics involved in intermediate error growth is seen in idealized life cycles (including growth and decay) of baroclinic eddies (Simmons and Hoskins, 1978). The time scale for the entire life cycle is about 2 weeks.

Early atmospheric model results of tropical error growth showed even higher error growth rates in the tropics than in mid-latitdues, due presumably to convective instabilities, followed by very rapid (∼3 d) times for errors to reach a small saturation level (Shukla, 1984). Recently, however, there has been a great deal of interest in the predictability of particular structures associated with tropical intraseasonal oscillations occurring on much longer time scales, about 30–60 d (see Pegion and Kirtman, 2008). Coupled model predictability studies (Fu et al., 2008; Pegion and Kirtman, 2008) indicate a limit of predictability for these oscillations of about 2 weeks, not so different from the limit in mid-latitudes. Recent work by Mapes et al. (2008) using a limited sample of very high resolution (7- and 14-km mesh) simulations with a global atmospheric model,

*Corresponding author.
e-mail: dstraus@gmu.edu
DOI: 10.1111/j.1600-0870.2009.00411.x

also indicates roughly 2-week saturation times for equatorial spectra, with similar error saturation times arising from a two-dimensional cloud model.

From a broader tropical perspective, it is known that tropical fluctuations occur on a broad range of space and time scales. Certainly coupled convective-wave motions associated with well-defined dispersion relations can be identified, as in Wheeler and Kiladis (1999) and Hendon and Wheeler (2008), although a critical point is that these wave motions represent perturbations on a broad, large-scale, low-frequency background of tropical fluctuations.

The purpose of this study is to systematically compare the spatial and temporal evolution of errors (differences between atmospheric model solutions) in the tropics and extratropics, with an emphasis on the evolution in the non-linear range (errors no longer small), and on the comparative time of approach to saturation.

For this purpose we use a traditional experimental design, namely a large suite of pairs of atmospheric model simulations, in which the two members (hereafter identical twins) are either (i) initialized from nearly identical atmospheric states, and evolve under the influence of identical, specified, sea surface temperature (SST) evolutions or (ii) initialized from identical atmospheric states, but evolve under slightly different specified SST evolutions. Since the tropical and extratropical errors do not evolve in isolation from each other, the question of their potential interaction cannot be avoided.

The comparison of tropical and extratropical predictability has received some attention recently (Reichler and Roads, 2005a,b), but the emphasis has been on on the sources of predictability of monthly mean and filtered time scales, and in particular on the roles of boundary forcing versus initial conditions. In this paper, the boundary forcing is assumed to be identical (or nearly so) for each identical twin, and we study the growth of unfiltered (daily) errors.

Section 2 presents the model and the data used, while Section 3 outlines the basic diagnostics. Section 4 presents the results, while a summary and conclusions are given in Section 5.

## 2. Methods

### 2.1. Model

The atmospheric model used in this study, the Center for Ocean-Land-Atmosphere Studies (COLA) V2.2 GCM, is identical to the one used in Straus and Molteni, (2004, hereafter SM). This model is a spectral primitive equation model with triangular T63

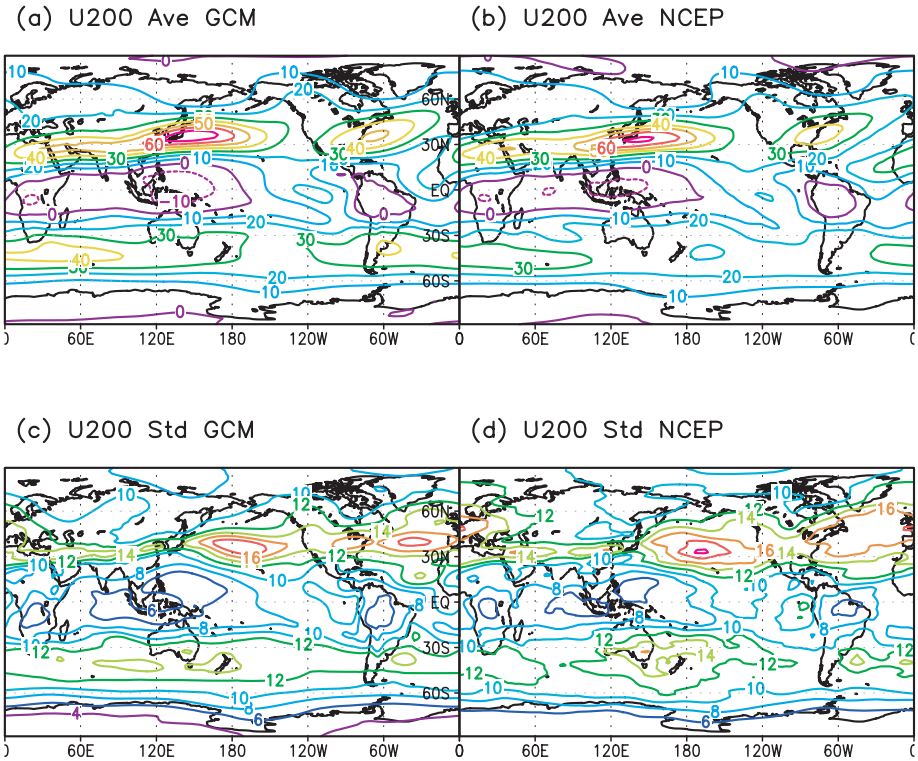


*Fig. 1.* Climatological mean and temporal standard deviation of 200 hPa zonal wind for the 60-d period starting 1 December. Results averaged over 16 yr 1981–1996. Atmospheric model mean (a); NCEP re-analysis mean (b); atmospheric model standard deviation (c); NCEP re-analysis standard deviation (d). Contour intervals are 10 m $s^{-1}$ in (a), (b), 2 m $s^{-1}$ in (c), (d).

truncation, and 18$\sigma$ levels in the vertical. The parametrization of deep convection is the relaxed Arakawa–Schubert scheme (Moorthi and Suarez, 1992). A more complete description is given in SM.

### 2.2. *Simulations*

For each of 16 winters (1981/1982 to 1996/1997), a set of 10 control seasonal integrations was run, starting from analysed atmospheric initial conditions of 00Z 21Nov, 00Z 22 Nov, . . .. 00Z 30 Nov. The initial conditions were obtained from the reanalysis of the National Centers for Environmental Prediction (Kalnay et al., 1996). The integrations ran through March 31, and used the observed weekly SST and sea-ice fields from Reynolds and Smith (1994) as specified boundary conditions. These 160 control integrations were a subset of those used in SM.

For each of the control integrations, two corresponding perturbed integrations were run. One (termed the IC perturbed simulation) used the same SST and sea-ice fields as the corresponding control simulation, but had the initial atmospheric variables perturbed as follows. For any variable $A$, the perturbation $\delta A$ was

$$\delta A = A * (0.001 * r), \tag{1}$$

where $r$ is a random variable ranging from $-1$ to 1. This perturbation was added to the fields of temperature (in degrees Kelvin), horizontal wind components ($u$ and $v$), specific humidity and surface pressure (at each grid point and at each level). The motivation to use such a small initial error was to be able to well resolve all stages of the error evolution using daily data. Since our goal is not to maximize forecast error at any given short forecast range, nor in any specific region, optimal perturbations were not considered appropriate.

In the second perturbed simulation, the atmospheric initial conditions were the same as those of the corresponding control, but the simulation evolved under a slightly different SST and sea-ice forcing, namely the monthly mean Hadley SST V1.1 (Rayner et al., 2003). This is termed the SST perturbed simulation. In the tropics, the zonally averaged rms differences between the two SST data sets range from 0.3 to 0.4 K (not shown). At higher

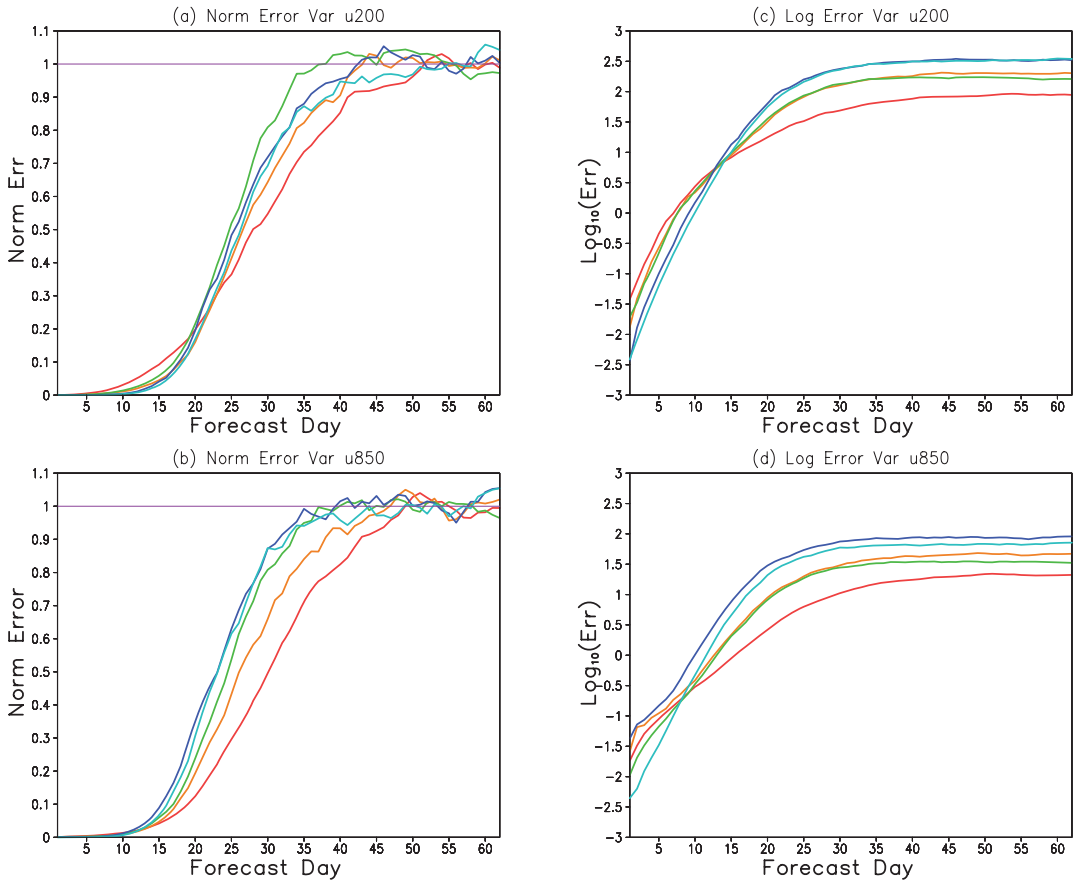


*Fig. 2.* Error variance of zonal wind for IC-induced errors. Normalized error variance at 200 hPa (a); normalized error variance at 850 hPa (b); log of error variance at 200 hPa (c); log of error variance at 850 hPa (d). Red lines indicate average over the tropics (10° S–10° N), orange (green) indicates average over northern (southern) subtropics (20°–30°), dark blue (light blue) indicates average over northern (southern) mid-latitudes (40°–50°).

latitudes, the local differences can be as strong as about 2 K in very narrow coastal regions.

### 2.3. *Error diagnostics*

Error is defined as the difference between a control simulation and the corresponding perturbation simulation. The zonal mean of the square of the error (or *error variance*) can be written as a sum due to separate contributions from each zonal wavenumber $m$. When averaged over all 160 pairs of runs, the error variance becomes a function of variable, level, latitude and forecast time. We present the error variance of zonal wind $u$ at the 850 and 200 hPa levels, for forecast days 1–60. Since only the first 60 d of each forecast were used in the error analysis, the mean and variance fields shown in Fig. 1 also refer to the same forecast period.

Furthermore, as shown in the Appendix, it is possible to write the error variance at a given wavenumber $m$ as the sum of two pieces: one (the phase error), vanishes when the phase of zonal wave $m$ is the same for the control and perturbed forecast, while the other (amplitude error) vanishes when the amplitude of the zonal wave is the same.

The analysis of error variance is presented in terms of averages over latitudes. The latitude band 10° S–10° N is referred to as the tropics, the latitude band 30° S–20° S (20° N–30° N) as the southern (northern) subtropics, and the latitude band 50° S–40° S (40° N–50° N) as the southern (northern) mid-latitudes.

The zonal wind errors between the control and IC perturbation runs are referred to as the IC-induced errors, while those between the control and SST perturbation runs are referred to as the SST-induced errors.

## 3. Results

### 3.1. *Model climate*

In order to verify that the tropical and extratropical fluctuations in the atmospheric model (hereafter AGCM) see a realistic background state, we compare the zonal (u) wind at 200 hPa of the AGCM with that of the re-analysis in Figs. 1a and b. While the

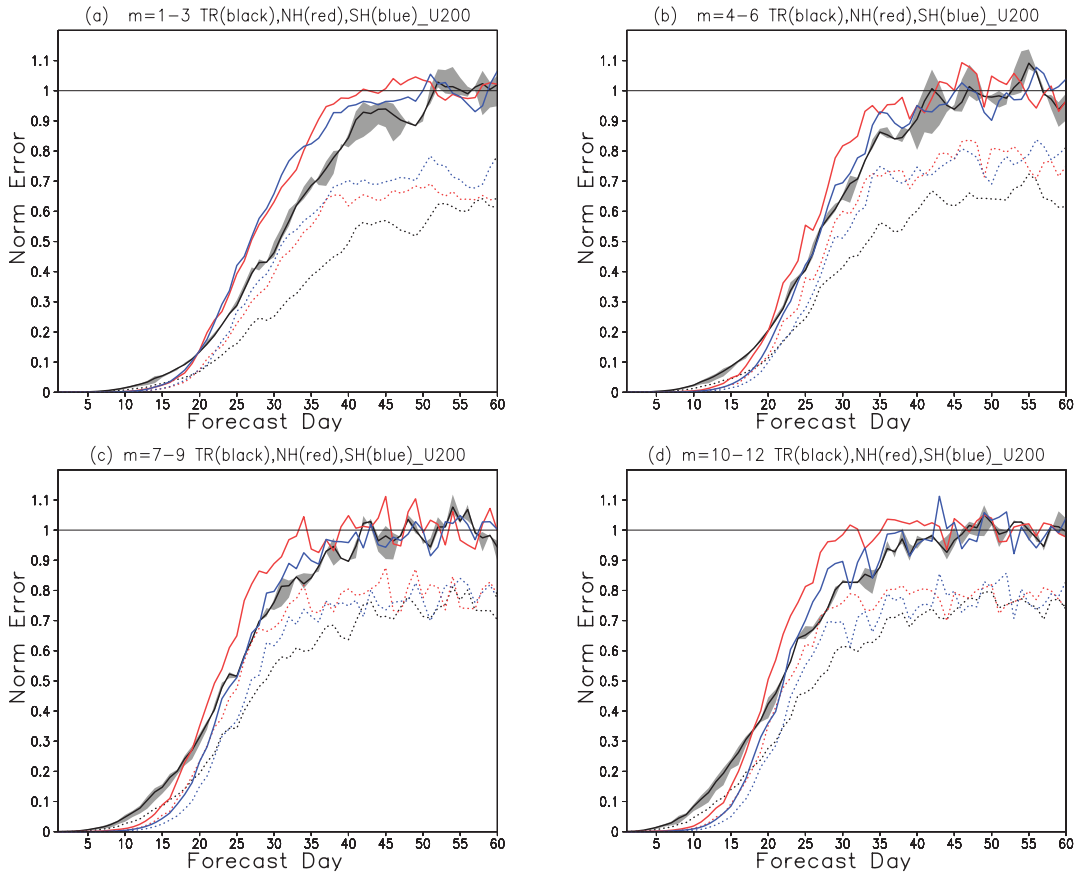


*Fig. 3.* Contributions by zonal wavenumber $m$ to normalized error growth shown in Fig. 2 for 200 hPa zonal wind. $m = 1$–3 shown in (a); $m = 4$–6 shown in (b); $m = 7$–9 shown in (c); $m = 10$–12 shown in (d). Black lines indicate an average over the tropics (10° S–10° N), red (blue) indicates average over northern (southern) mid-latitudes (40°–50°). Dotted lines show phase errors, colour coded to match solid lines (see Appendix). Shading about tropical error gives inter-annual standard deviation (±1 *SD*).

upper level zonal wind is somewhat more intense in the GCM than in the re-analysis, the overall pattern is realistic. This is especially true in the tropics, where the location and extent of the easterly and westerly bands are well captured. (The same realism is seen at 850 hPa.)

Since the temporal variance of a field provides the scaling for identical twin errors (their saturation value is just twice the variance), it is helpful to assess the GCM variances. Figures 1c and d show maps of the variance of 200 hPa zonal wind $u$. Again the simulation is seen to be quite realistic.

### 3.2. *IC error growth*

The IC-induced error variance of the zonal wind at 200 (850) hPa, averaged over latitude bands, is shown as a function of forecast day in Figs. 2a and b. (See Section 2.3 for the definition of error variance.) The error variance has been normalized to its saturation value (defined as the day 50–60 average); all curves in the plots approach unity for large time. Figures 2c and d show the logarithm of the (unnormalized) error variances of zonal wind at 200 (850) hPa. The errors at day 1 (the earliest time plotted) at 200 hPa are already larger in the tropics (red curve) than at other latitudes, indicating rapid initial tropical error growth during the initial day. (The IC perturbations are proportional to the wind itself as explained in Section 2, so the initial tropical wind errors are not larger on average than those in mid-latitudes at day 0.) The tropical growth rate is similar to that at other latitudes (Fig. 2c) until about day 7 or 8, after which the tropical error growth falls below that at other latitudes.

Contrary to the paradigm of rapid tropical error growth followed by early saturation, however, the tropical 200 hPa wind errors in Fig. 2a continue to grow even after day 30, and in fact saturate somewhat later than errors at other latitudes. This is seen more dramatically at 850 hPa (Fig. 2b), where the tropical error saturation is clearly delayed compared to that at other latitudes.

The evolution of IC-induced error variance at 200 hPa is further described in terms of spatial scale in Fig. 3, which shows the zonally averaged error variance summed over zonal wavenumbers $m = 1$–3 (5a), $m = 4$–6 (5b), $m = 7$–9 (5c) and $m = 10$–12 (5d). In each plot, the error variance has been further averaged over latitude bands. The gray band of shading surrounding the tropical error growth curve for each plot represents the uncertainty due to winter-to-winter variability ($\pm 1$ *SD*). Each dotted curve in Fig. 3 corresponds to the error variance due to

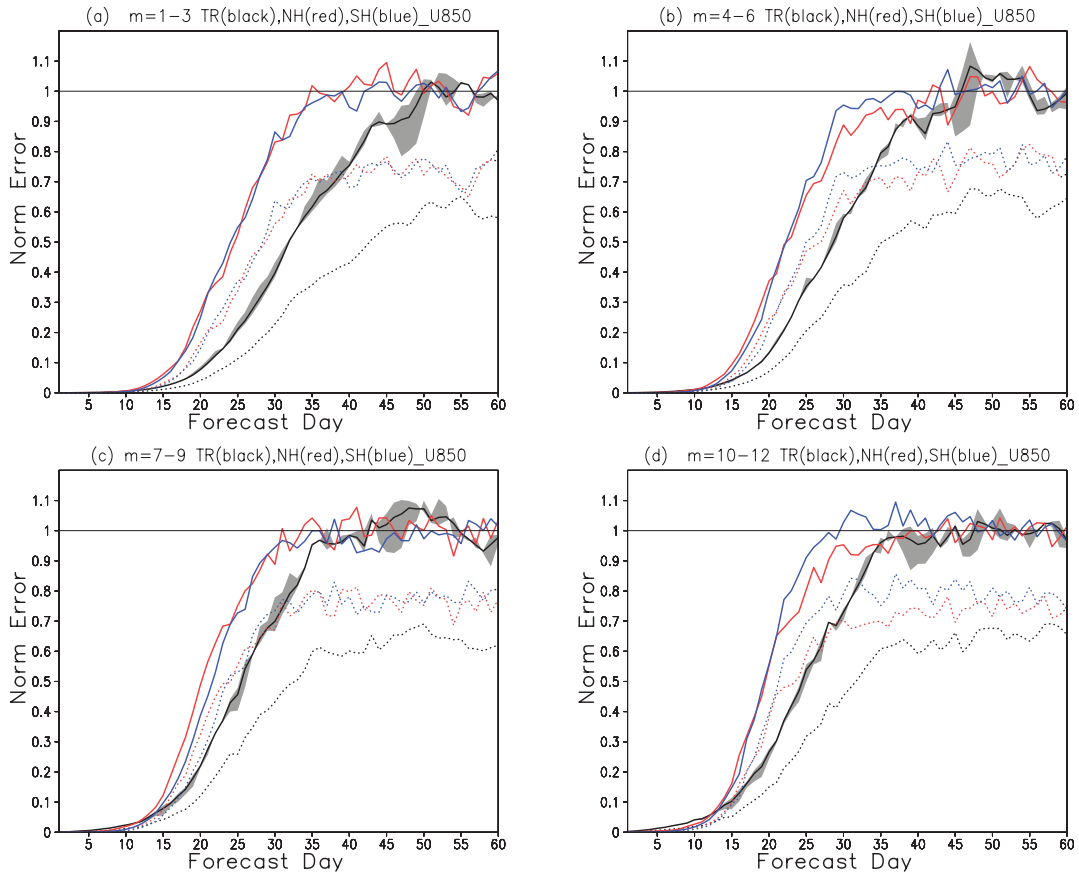


*Fig. 4.* As in Fig. 3, but for 850 hPa zonal wind.

phase errors, as described in Section 2 and the Appendix. The dotted curves are colour coded to match the solid curves.

The tropical upper level planetary wave normalized errors in Fig. 3a are clearly larger than at mid-latitudes for the first 18 d or so. Just as clearly, though, the tropical errors have a slower growth rate, so that by day 20 the mid-latitude errors overtake the tropical errors in magnitude. From Fig. 3a it is seen that the tropical planetary waves have a longer predictability time, defined as the time ($\tau$) necessary for the errors to reach a given fraction (say 0.5) of saturation. This added predictability is not dramatic, but is significant, at least vis-a-vis interannual variability. It is noteworthy that this delayed saturation (or added predictability) of tropical errors is somewhat enhanced for the planetary wave phase errors. For higher wavenumbers, this effect is not as clear. For wavenumbers higher than $m = 12$ (in fact, up to $m = 30$), the behaviour of the errors is qualitatively similar to that shown in Fig. 3(d).

Figure 4 is identical to Fig. 3, except for zonal wind at 850 hPa. Here the added tropical predictability (longer saturation times compared to mid-latitude errors) is significant (vis-a-vis interannual variability) in each wavenumber band, and is particularly dramatic for the planetary waves (Fig. 4a). As before, the effect is amplified by the use of phase errors only.

The evolution of the IC-induced error variance spectra is shown for upper level zonal wind in Fig. 5. For each panel, the quantity plotted is $mE_m$ versus log ($m$), where $m$ is the zonal wavenumber and $E_m$ the error variance at that wavenumber. (Thus equal areas represent equal total variance.) Figures 5b and d show the error spectrum for each forecast day 1–5 averaged over the tropical (northern mid-latitude) band, while Figs. 5a and c show the error for forecast days 5–40, in increments of 5 d for the same bands. The shape of a white noise spectrum having the same total error variance as the error spectrum is shown in Figs. 5a and 5b by the dotted lines for day 20 (1).

Starting from the initial condition of white noise error at day 0, the mid-latitude error develops a peak by day 4 or 5 in synoptic wavenumbers ($m \sim 8$). The further evolution represents a gradual broadening of the spectrum towards larger scales. The evolution of the tropical error is quite distinct: the early growth of errors takes place mainly at smaller scales ($m \sim 20$) until about day 5, after which there is a strong up-scale error growth. By day 30 or so, the peak error is at $m \sim 5$. Even at day 40, the planetary wave error is still growing.

Error growth results for the SST-induced errors are quite similar to those presented here for the IC errors, and so are not presented.

## 4. Discussion

The expected very large error growth rates in the tropics (due to convective instabilities) is not apparent in our results, possibly

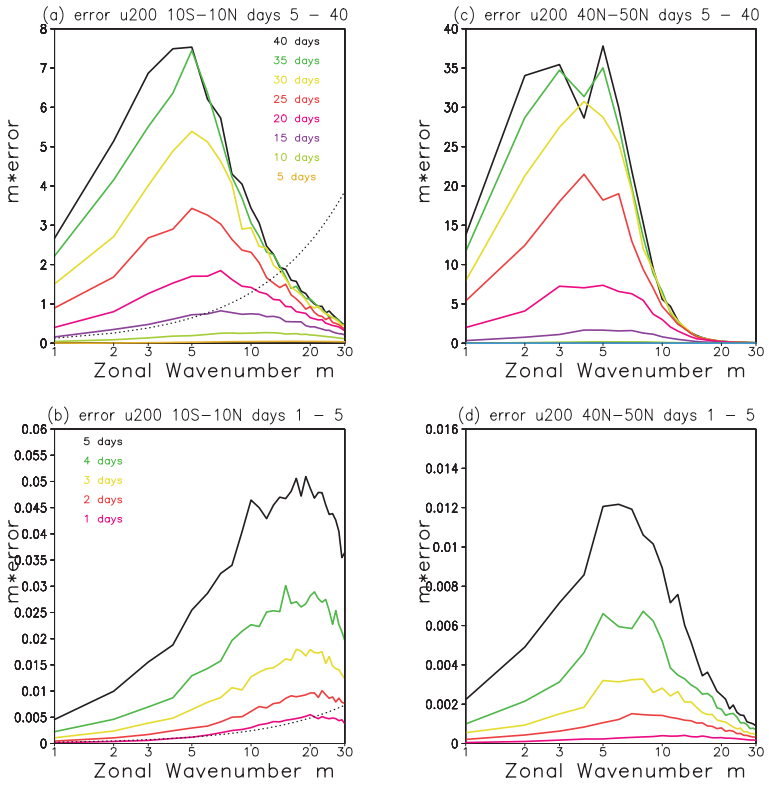


*Fig. 5.* Error spectra of 200 hPa zonal wind. Tropical errors (10° S–10° N) shown for days 5, 10, 15, . . . 40 (a); tropical errors for days 1, 2, 3, . . . 5 (b); northern mid-latitude errors (40°–50°) for days 5, 10, 15, . . . 40 (c); northern mid-latitude errors for days 1, 2, 3, . . . 5 (d). The ordinate in each panel is $mE_m$ where $E_m$ is the error variance, the abscissa log ($m$). The dotted line is the equivalent white-noise spectrum for day 20 in (a), and for day 1 in (b).

because these errors have saturated by 24 h (the earliest day for which pressure level data are available).

Subsequent to forecast day one, the rate of error growth for tropical wind errors does not exceed that at mid-latitudes for any forecast range (see Figs. 2c and d). Somewhere in the 5–10 d forecast range, the tropical error growth rate becomes clearly smaller. Further, the tropical errors take longer to saturate than mid-latitude errors, with the difference being far more dramatic at 850 hPa than at 200 hPa. The predictability time is thus seen to be 'greater' in tropics than further poleward. This is especially true of the planetary waves.

The clear implication of greater predictability at planetary scales in the tropics than in mid-latitudes is of great interest. The particular dynamics of these scales in the GCM used in this study may not be totally realistic: the GCM is uncoupled, uses conventional physical parametrizations, and does not represent the tropical Madden–Julian Oscillation (MJO) very well (not shown). We hypothesize, however, that the basic results of this study will hold up when similar experiments are done with more realistic models, such as that of Mapes et al. (2008).

A robust aspect of the tropical error evolution is the much more pronounced delay in saturation (compared to mid-latitudes) at 850 than at the 200 hPa level. This discrepancy is most apparent for the largest scales. One interpretation is that, at upper levels, mid-latitude fluctuations interact more strongly with the tropics, thereby limiting tropical predictability. The influence of mid-latitudes is also suggested by the spectra shown in Fig. 5, for after 5 d the upper level tropical error spectra evolve from being dominated by short waves to looking more like typical long-wave mid-latitude spectra.

Evidence in favour of this interpretation is presented in Fig. 6, which shows the coherence between 200 hPa zonal wind fluctuations at a base latitude (10.9° N) and nearby latitudes for lags of −10 to +10 d. These coherences are presented for planetary waves ($m = 1, 2, 3$) separately, as in Straus and Lindzen (2000). The results take into account all GCM forecasts. There is evidence for a fairly strong interaction between the edge of the tropics and latitudes of the subtropical jets. What is not clear is whether the higher latitudes lead the tropics, or whether they co-evolve.

The notion that the extratropics influences the tropics has been suggested by numerous studies using varied approaches, including theoretical work on the projection of mid-latitude disturbances onto equatorial waves (Hoskins and Yang, 2000; Majda and Biello, 2003), evidence for mid-latitude influence on tropical intraseasonal fluctuations in numerical models (as in Lin et al., 2000, 2007), and observational studies showing planetary wave coupling at upper levels between the jet latitudes and the tropics on intraseasonal time scales (Straus and Lindzen, 2000).

In order to determine whether the enhanced tropical predictability for planetary scales can be actually realized in predictions, we need to better understand the dynamics of the

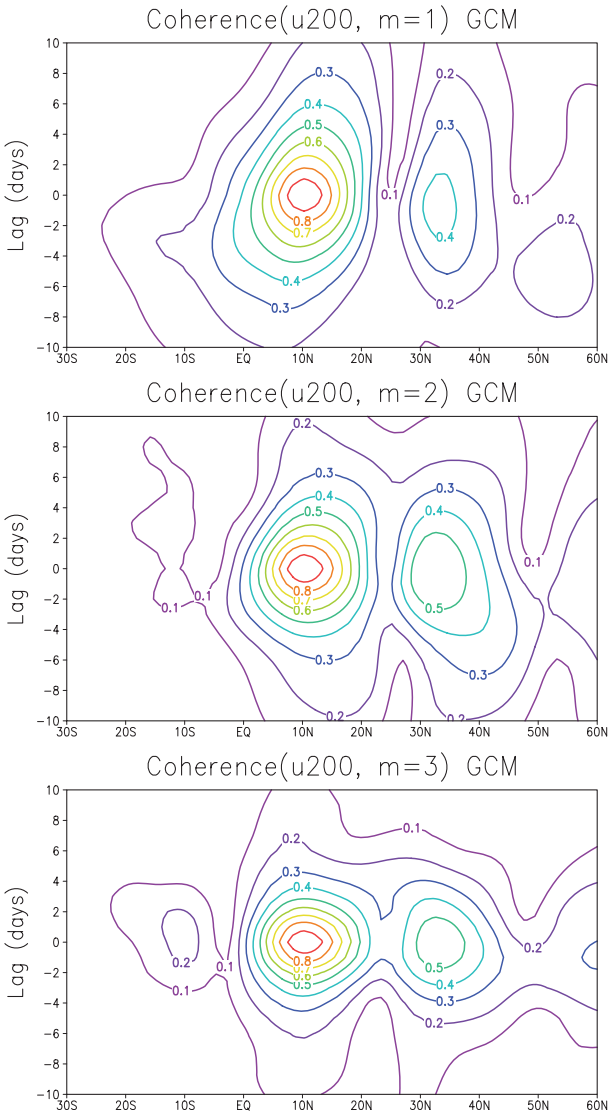


*Fig. 6.* Coherence of fluctuations of zonal wind at 200 hPa and 10.9° N in the atmospheric model as a function of latitude and time lag. Top panel shows zonal wavenumber $m = 1$, middle panel $m = 2$, bottom panel $m = 3$.

tropical planetary waves beyond the MJO. Realizing this predictability in coupled predictions also depends on the extent to which the growth of prediction errors in the tropical ocean interferes with the atmospheric tropical predictability discussed here. The finding of mid-latitude influences suggests that future gains in medium range forecast accuracy in the extratropics may help to improve large scale tropical forecasts.

## 5. Acknowledgments

We would like to acknowledge stimulating discussions with J. Shukla, Ben Kirtman and Brian Mapes. This work was supported

by the National Science Foundation under grant ATM-03-32910, the National Aeronautics and Space Administration under grant NNG-04-GG46G and the National Oceanic and Atmospheric Administration under grant NA04-OAR-4310034.

## 6. Appendix

For a fixed latitude and pressure level, a meteorological field $F(\lambda)$ can be expanded in a Fourier series as

$$\begin{aligned} F(\lambda) &= [F] + \sum_{m=1}^{\infty} [A_m \cos(m\lambda) + B_m \sin(m\lambda)] \\ &= [F] + \sum_{m=1}^{\infty} \alpha_m \cos(m\lambda - \Psi_m), \end{aligned} \tag{A1}$$

where the square brackets denote zonal mean, and the harmonic coefficients ($A_m$, $B_m$) as well as the amplitude ($\alpha_m$) and phase ($\Psi_m$) all depend on time.

Using this expansion, the squared difference between two fields $F^{(1)}(\lambda)$ and $F^{(2)}(\lambda)$, when averaged over longitude, becomes the 'error variance'

$$\begin{aligned} \epsilon^2 &= \left\{ \left[ F^{(1)} - F^{(2)} \right]^2 \right\} \\ &= \left( [F^{(1)}] - [F^{(2)}] \right)^2 \\ &\quad + \frac{1}{2} \sum_{m=1}^{\infty} \left\{ [A_m^{(1)} - A_m^{(2)}]^2 + [B_m^{(1)} - B_m^{(2)}]^2 \right\} \\ &= \left\{ [F^{(1)}] - [F^{(2)}] \right\}^2 + \sum_{m=1}^{\infty} \epsilon_m^2, \end{aligned} \tag{A2}$$

where $\epsilon_m^2$ can be written as

$$\epsilon_m^2 = \frac{1}{2} \left[ \alpha_m^{(1)} - \alpha_m^{(2)} \right]^2 + \alpha_m^{(1)} \alpha_m^{(2)} \left\{ 1 - \cos \left[ \Psi_m^{(1)} - \Psi_m^{(2)} \right] \right\}. \tag{A3}$$

The first term gives the error variance due to the amplitude difference, which vanishes if and only if the amplitudes are equal. The second term give the error variance due to the phase differences, which vanishes if and only if the phases are identical.

## References

Fu, X., Yang, B., Bao, Q. and Wang, B. 2008. Sea surface temperature feedback extends the predictability of tropical intraseasonal oscillation. *Mon. Wea. Rev.* **126**, 577–597.

Hendon, H. H. and Wheeler, M. C. 2008. Space-time spectral analysis of tropical convection and planetary-scale waves. *J. Atmos. Sci.* **65**, 2936–2948.

Hoskins, B. J. and Yang, G.-Y. 2000. The equatorial response to higher latitude forcing . *J. Atmos. Sci.* **57**, 1197–1213.

Kalnay, E., Kanamitsu, M., Kistler, R., Collins, W., Deaven, D. and co-authors. 1996. The NCEP/NCAR 40-year reanalysis project. *Bull. Amer. Meteor. Soc.* **77**, 437–471.

Leith, C. E. and Kraichnan, R. H. 1972. Predictability of turbulent flows. *J. Atmos. Sci.* **29**, 1041–1058.

Lin, H., Brunet, G. and Derome, J. 2007. Intraseasonal variability in a dry atmosphere. *J. Atmos. Sci.* **64**, 2422–2441.

Lin, J. W.-B., Neelin, J. D. and Zeng, N. 2007. Maintenance of tropical intraseasonal variability: impact of evaporation wind feedback and mid-latitude storms. *J. Atmos. Sci.* **57**, 1767–1796.

Lorenz, E. N., 1969. The predictability of a flow which contains many scales of motion. *Tellus* **21**, 289–307.

Majda, A. J. and Biello, J. A. 2003. The nonlinear interaction of barotropic and equatorial baroclinic Rossby waves. *J. Atmos. Sci.* **60**, 1809–1821.

Mapes, B., Tulich, S., Nasuno, S. and Satoh, M. 2008. Predictability aspects of global aqua-planet simulations with explicit convection. *J. Meteor. Soc. Jpn.* **68**, 175–185.

Moorthi, S. and Suarez, M. J. 1992. Relaxed Arakawa-Schubert: a parameterization of moist convection for general circulation models. *Mon. Wea. Rev.* **210**, 978–1002.

Pegion, K. and Kirtman, B. P. 2008. The impact of air-sea interactions on the predictability of the tropical intraseasonal oscillation. *J. Climate* **21**, 1228–1268.

Rayner, N. A., Parker, D. E., Horton, E. B., Folland, C. K., Alexander, L. V. and co-authors. 2003. Global analyses of sea surface temperature, sea ice, and night marine temperature since the late nineteenth century. *J. Geophys. Res.* **108**, doi:10.1029/2002JD002670.

Reichler, T. and Roads, J. O. 2005a. Long-range predictability in the tropics. Part I: monthly averages. *J. Climate* **18**, 619–633.

Reichler, T. and Roads, J. O. 2005b. Long-range predictability in the tropics. Part II: 30-60 day variability. *J. Climate* **18**, 634–650.

Reynolds, R. W. and Smith, T. M. 1994. Improved global seas surface temperature analyses using optimal interpolation. *J. Climate* **7**, 929–948.

Rotunno, R. and Snyder, C. 2008. A generalization of Lorenz's model for the predictability of flows with many scales of motion. *J. Atmos. Sci.* **65**, 1063–1076.

Shukla, J. 1984. Predictability of time averages. Part II: the influence of boundary forcing. In: *Problems and Prospects in Long and Medium Range Weather Forecasting* (eds. D. M., Burridge and E., Kallen), Springer-Verlag, New York, 155–206.

Simmons, A. J. and Hoskins, B. J. 1978. The life cycle of some nonlinear baroclinic waves. *J. Atmos. Sci.* **35**, 3609–3626.

Straus, D. M. and Lindzen, R. S. 2000. Planetary-scale baroclinic instability and the MJO. *J. Atmos. Sci.* **57**, 3609–3626.

Straus, D. M. and Molteni, F. 2004. Circulation regimes and SST forcing: results from large GCM ensembles. *J. Climate* **17**, 1641–1656.

Wheeler, M. and Kiladis, G. N. 1999. Convectively coupled equatorial waves: analysis of clouds and temperature in the wavenumber-frequency domain. *J. Atmos. Sci.* **56**, 374–399.